High Fidelity Physics Simulation of 128 Channel MIMO Sensor for 77GHz Automotive Radar

USHEMADZORO CHIPENGO, (Student Member, IEEE), ARIEN SLIGAR, AND SHAWN CARPENTER
Ansys Inc., Canonsburg, PA 15317, USA

Corresponding author: Ushemadzoro Chipengo (ushe.chipengo@ansys.com)

ABSTRACT Automotive radar is one of the enabling technologies for advanced driver assistance systems (ADAS) and subsequently fully autonomous vehicles. Along with determining the range and velocity of targets with fairly high resolution, autonomous vehicles navigating complex urban environments need radar sensors with high azimuth and elevation resolution. Size and cost constraints limit the physical number of antennas that can be used to achieve high resolution direction-of-arrival (DoA) estimation. Multiple-input/multiple-output (MIMO) schemes achieve larger virtual arrays using fewer physical antennas than would be needed for a single-input/multiple-output (SIMO) system. This paper presents a high-fidelity physics simulation of a 77GHz, frequency-modulated continuous-waveform (FMCW)-based 128 channel (8 transmitters (T_x), 16 receivers (R_x)) MIMO radar sensor. The 77GHz synthetic radar returns from full scale traffic scenes are obtained using a high-fidelity physics, shooting and bouncing ray electromagnetics solver. A fast Fourier transform (FFT) based signal processing scheme is used across slow-time (chirp) and space (channel) to obtain range-Doppler and DoA maps, respectively. Detection and angular separation performance comparisons of 16, 64 and 128 channel MIMO radar sensors are made for two complex driving scenarios.

INDEX TERMS Automotive radar, antenna, MIMO, FMCW, simulation, DoA.

I. INTRODUCTION

Advanced driver assistance systems (ADAS) have turned today's vehicles into mobile computing and sensing hubs that will ultimately, autonomously navigate roads as self driving cars. One of the main demands of autonomous operation is that the vehicle under consideration must have situational awareness. Here, we define the host vehicle that is tasked with perceiving the environment using the on-board sensors as the ego vehicle. Specifically, the ego vehicle must be able to detect the presence, distance, speed and direction of arrival of multiple actors in the driving scenario. This is achieved using different sensing technologies such as light detection and ranging (Lidar), range detection and ranging (radar), visible spectrum cameras and ultrasonic proximity sensors [1]–[4]. Radar is a versatile technology that can detect the range, velocity and direction of arrival of multiple targets simultaneously in poor lighting conditions and inclement weather [5].

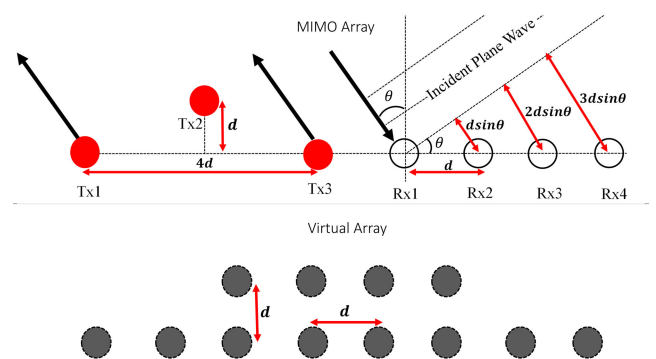The associate editor coordinating the review of this manuscript and approving it for publication was Pia Addabbo.

FIGURE 1. Direction of arrival (DOA) estimation using the MIMO concept. Using 3 T_X antennas and 4 R_X antennas, a 12 channel virtual array can be realized for azimuth and elevation angle estimation.

Recent implementations of radar in the automotive industry have been focused on the 77 GHz frequency band. Here, radar is used for park-assist (PA), blind spot detection (BSD), rear collision warning (RCW), cross traffic alert (CTA) and adaptive cruise control (ACC), among others [6]. These different applications can be divided into long (ACC), medium (CTA, RCW and BSD) and short (PA) range radar. In highway
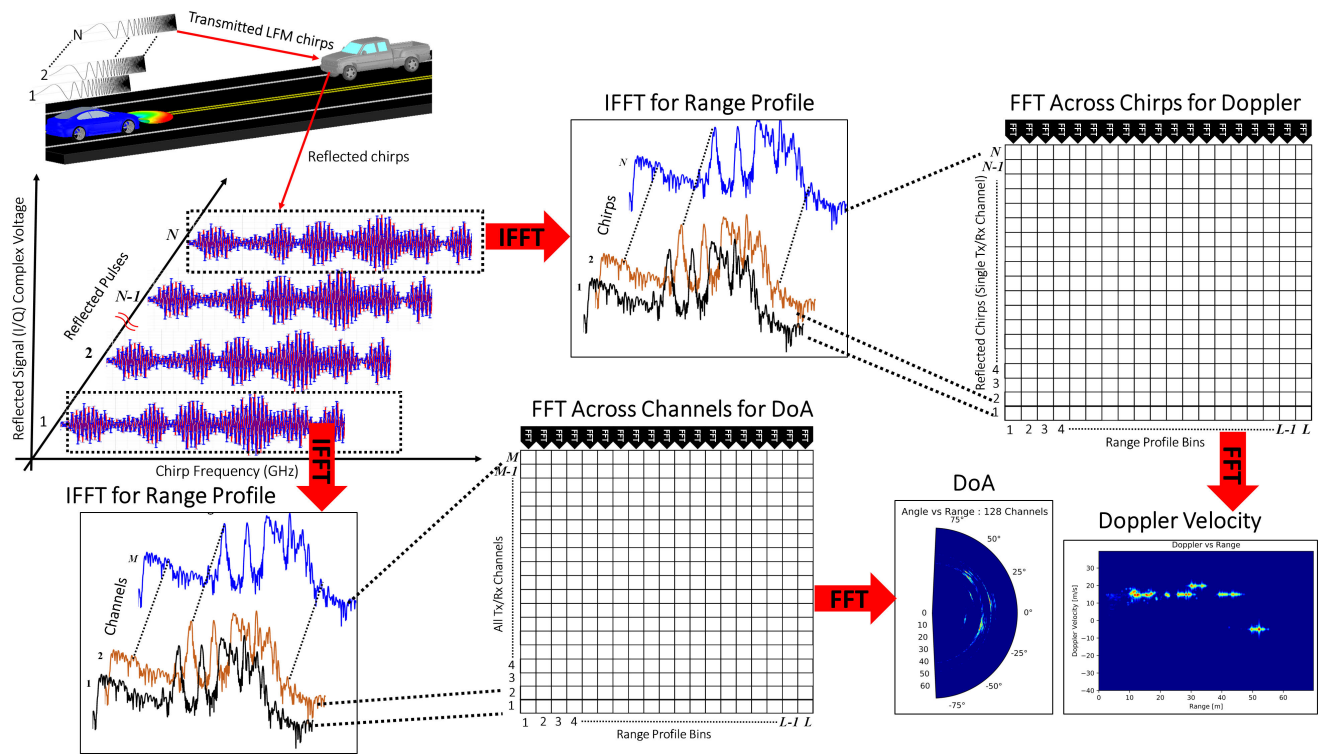
FIGURE 2. FFT based signal processing workflow for range, Doppler and angle. A range profile is obtained through a 1D IFFT along fast-time. Range-Doppler and angle are obtained using FFTs along chirps (slow-time) and channels, respectively.

operation, long range radars are used to track the distance and velocity of relatively few targets that have a smaller dynamic range in radar cross section (RCS) [7]. Urban environments present unique challenges to radar sensor operation. Here, the sensor must detect, track and classify multiple, crowded targets with relatively slow speeds and high dynamic ranges in RCS. Specifically, the RCS of a pedestrian can be 20 dB less than that of a truck [7]. In addition to separating targets in azimuth, targets must also be separated in elevation. This is because the radar sensor will need to accurately determine the position in elevation of targets such as small metallic pieces on the ground, manholes or overpasses in order to avoid a false detection [7], [8]. Medium and short range radars will need to operate in complex electromagnetic environments for fully autonomous vehicles (AV) to be realized.

To meet performance requirements, medium and short range radar sensors must have a wide field of view coupled with high range, azimuth, elevation and velocity resolution. Using a frequency-modulated continuous-waveform (FMCW) radar, the range resolution can be improved by increasing the bandwidth B of the transmitted chirp. On the other hand, the velocity resolution can be improved by increasing the coherent processing interval (CPI) duration. In order to determine the direction of arrival of a target in azimuth or elevation, two or more channels are needed. The angular resolution of the sensor can be improved by increasing the number of channels. In a single-input/multiple-output (SIMO) scheme, the number of channels can be increased by

adding more receivers (R_x). Each of these additional receivers will need a dedicated frequency mixer, amplifier and analog-to-digital converter (ADC).

Due to the space and cost constraints of automotive radar, SIMO schemes are seldom used for high angular resolution radar. Instead of a single transmitter T_x used in SIMO systems, multiple-input/multiple-output (MIMO) radar systems improve hardware efficiency by using multiple T_x elements. By judiciously spacing the elements, larger virtual arrays can be achieved using a smaller number of physical channels. Fig. 1 shows the MIMO concept.

The MIMO radar concept has been extensively investigated [7], [9]–[18]. MIMO radar with co-located antennas was investigated in [10]. On the other hand MIMO radars with widely separated antennas were investigated in [17]. Various works involving the building and testing of automotive radar systems have been presented in the literature [5], [7], [19]–[23]. A 77 GHz MIMO automotive radar was built and tested in [7]. While building and testing radar sensors is valuable, it can be cost and time prohibitive to build certain test cases that may be of interest to system designers. It has been estimated that 8.8 billion test-driving miles will be needed before autonomous vehicles are deemed safe for mainstream deployment [24]. Simulation has emerged as a practical, relatively inexpensive and safe approach for ADAS sensor validation [25]–[30].

In this paper, we present a high-fidelity physics based simulation of a 128 channel MIMO radar sensor for 77 GHz
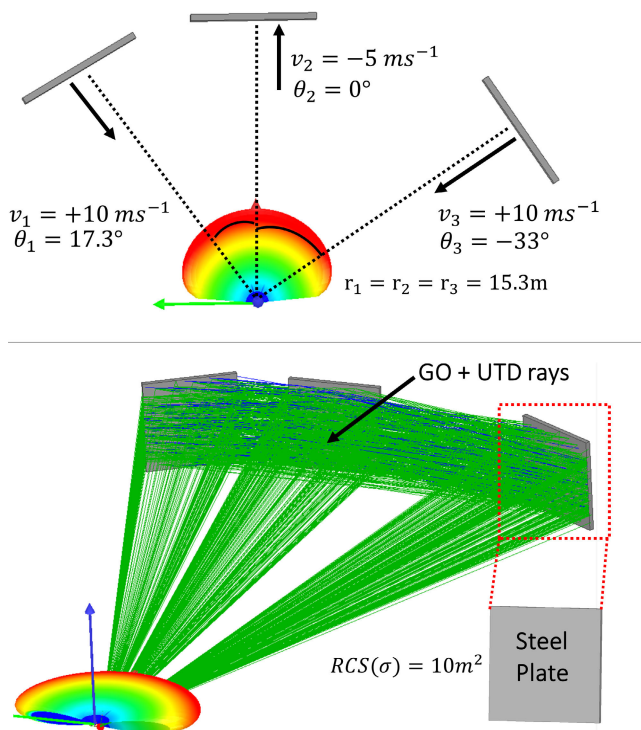
FIGURE 3. Simulation setup for validating the range, Doppler and angle estimation of the post processing technique used in this work. Each steel plate has a radar cross section of $10m^2$ at 77 GHz.

automotive radar. The synthetic radar sensor consists of 8 transmitter (T_x) and 16 receiver (R_x) elements. The radar signal is a frequency-modulated continuous-waveform (FMCW). Channel orthogonality is achieved through time domain multiplexing (TDM-MIMO). In TDM-MIMO, a single T_x antenna transmits while all the other T_x antennas are turned off. Doppler and angle processing of the scattered fields received by each of the R_x antennas is done using a fast Fourier transform (FFT) based scheme.

In order to test the performance of the MIMO sensor, the post processing algorithms need to be fed with synthetic radar returns obtained from electromagnetics simulations of full scale traffic scenes. The large electrical size of full scale traffic scenes makes it difficult to conduct simulations using the traditional full-wave electromagnetics solvers. Specifically, a single traffic scene can be billions of cubic wavelengths in size at 77GHz. This presents high computational and memory demands that are further increased by using MIMO sensors since individual T_x/R_x channels would need to be simulated. Therefore, electromagnetic simulations of full scale traffic scenes have been limited to low fidelity, analytical or system level models that treat targets as point scatterers and not distributed targets [27]–[33]. Such models typically neglect crucial wave propagation and multi-path interaction between accurate target shapes. In this work, the synthetic radar returns of full traffic scenes are obtained using Ansys'
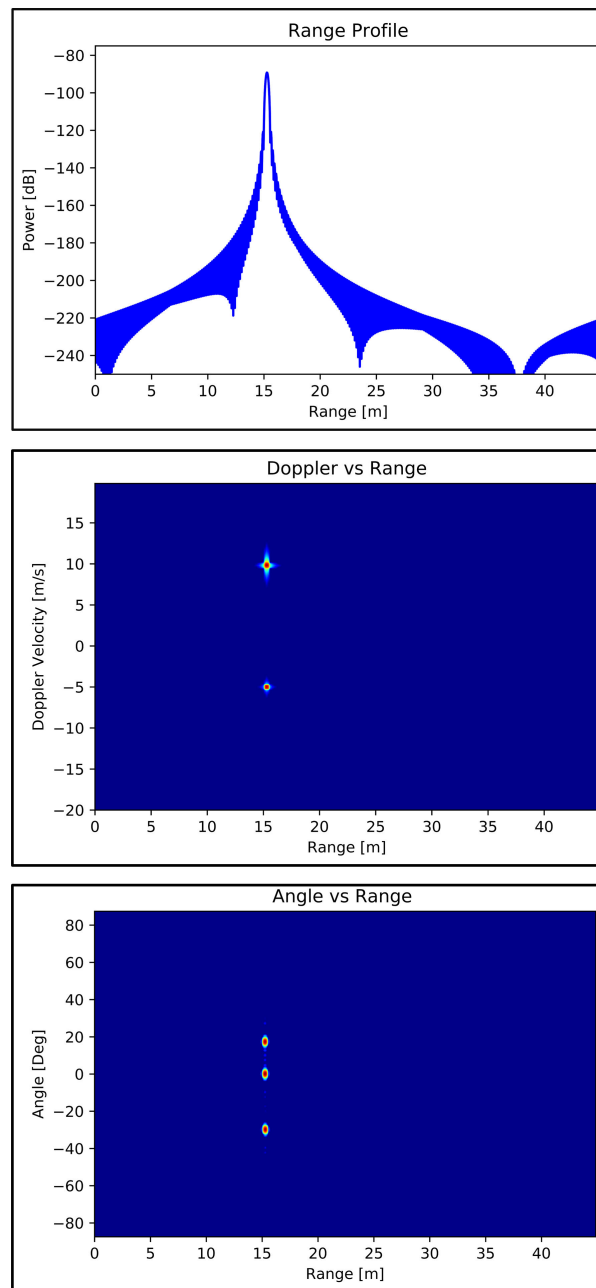

FIGURE 4. Range profile, range-Doppler map and range-angle map for the 3 steel-plate arrangement shown in Fig. 3 (128 channel MIMO array).

High Frequency Structure Simulator (HFSS) Shooting and Bouncing Rays solver (SBR+), a high-fidelity physics based ray tracing electromagnetics solver.

This paper is organized as follows: section II focuses on MIMO direction of arrival estimation theory and the FFT based signal processing scheme employed in this work. Section III presents the HFSS SBR+ simulation setup and a test case scenario used to validate the proposed simulation and post processing workflow. In section IV, two full scale traffic scenes of complex road scenarios are simulated to
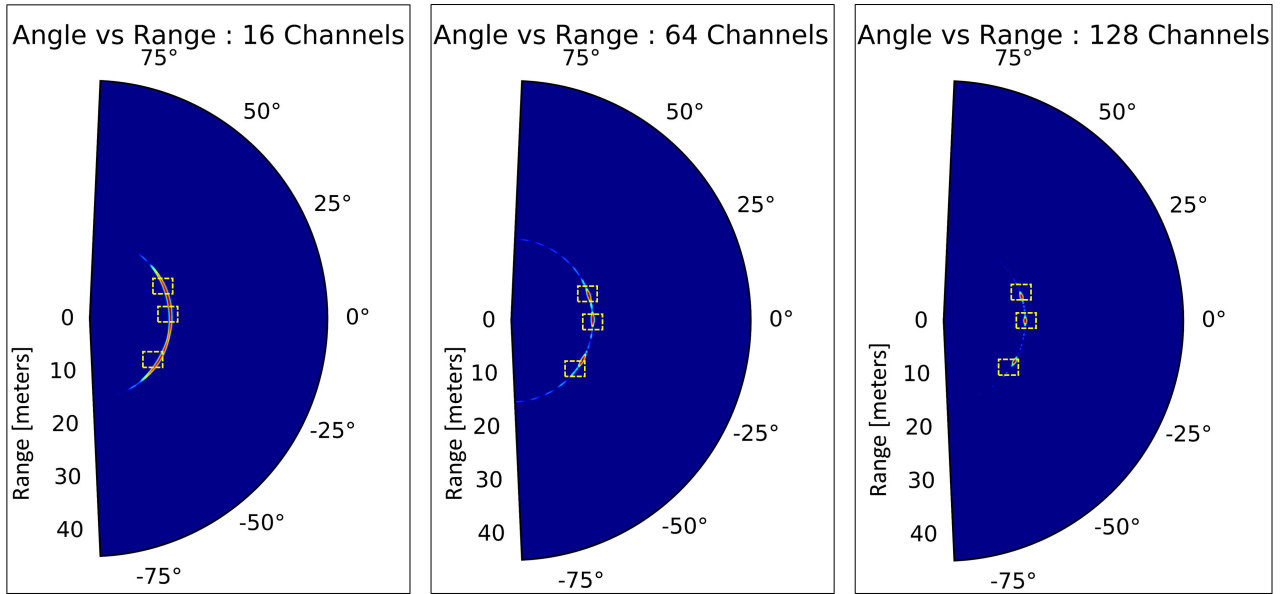
FIGURE 5. Range-angle maps for 16, 64 and 128 channels for the 3 steel-plate arrangement shown in Fig.3. The box shaped markers show the actual locations (range and angle) of the targets. Increasing the number of channels improves the DoA estimation resolution.

obtain range, velocity and angle of arrival of targets in the scene. For each of the scenes, the angle of arrival maps for 16, 64 and 128 channels are compared to determine the separability of targets for each case.

This paper has two main contributions. Here, we demonstrate how synthetic radar returns from a MIMO sensor can be extracted from a high-fidelity physics, full-scale electromagnetic simulation of traffic scenes for 77 GHz radar. To the authors' best knowledge, this is the first high-fidelity physics simulation demonstration of its kind. Secondly, we show how a simple, computationally efficient FFT scheme can be used to obtain range, Doppler and angle information from frequency domain synthetic radar returns. The workflow from this paper can be used to predict the performance of physical radar sensors in real world applications.

II. MIMO THEORY AND SYNTHETIC RADAR RETURNS POST PROCESSING

A. MIMO FOR DOA ESTIMATION

In order to determine the direction of arrival of a signal using a single-input/multiple-output (SIMO) system, at least two receiver antennas with a known physical separation are needed. This physical separation of receivers creates an angle-dependent phase shift between the signals received by the two receivers. Figure 1 shows an incoming plane wave at an angle θ. Each of the receiver antennas have a spacing of d, therefore, a single wave-front has to travel an additional physical distance of $(n-1)dsin\theta$ to reach the nth as shown in Fig. 1. Therefore, the signal at the receivers has a progressive phase shift, ϕ of

$$\phi = \frac{2\pi dsin\theta}{\lambda} \qquad (1)$$

Here, λ is the free space wavelength. Therefore, the angle of arrival is given by

$$\theta = sin^{-1}\left(\frac{\phi\lambda}{2\pi d}\right) \qquad (2)$$

The progressive phase shift ϕ can unambiguously be estimated in the range of $(-\pi$ to $\pi)$ radians. Therefore, this means that the field of view θ_{FOV} is given by

$$\theta_{FOV} = \pm sin^{-1}\left(\frac{\lambda}{2d}\right) \qquad (3)$$

By using a spacing $d = \lambda/2$, a field of view $\theta_{FOV} = \pm 90°$ can be achieved. The angular resolution of the DoA estimation θ_{RES} is given by

$$\theta_{RES} = \frac{\lambda}{Ndcos\theta} \qquad (4)$$

From (4), it can be seen that the angle of arrival estimation resolution depends on the number of antenna elements N, the distance between the elements d and the cosine of the angle of arrival estimation. This means that the angular resolution worsens as one moves from bore-sight ($\theta = 0°$). Assuming bore-sight conditions and a spacing $d = \lambda/2$, the angular resolution in radians is given by

$$\theta_{RES} = \frac{2}{N} \qquad (5)$$

By increasing the number of R_x elements in a SIMO scheme, the angular resolution can be improved. However, this is not an efficient usage of hardware since each receiver would need its own mixer, amplifier, filter and ADC. A more efficient way is to use a MIMO scheme as shown in Fig. 1. Here, we use M_{Tx} orthogonal waveforms from the phase
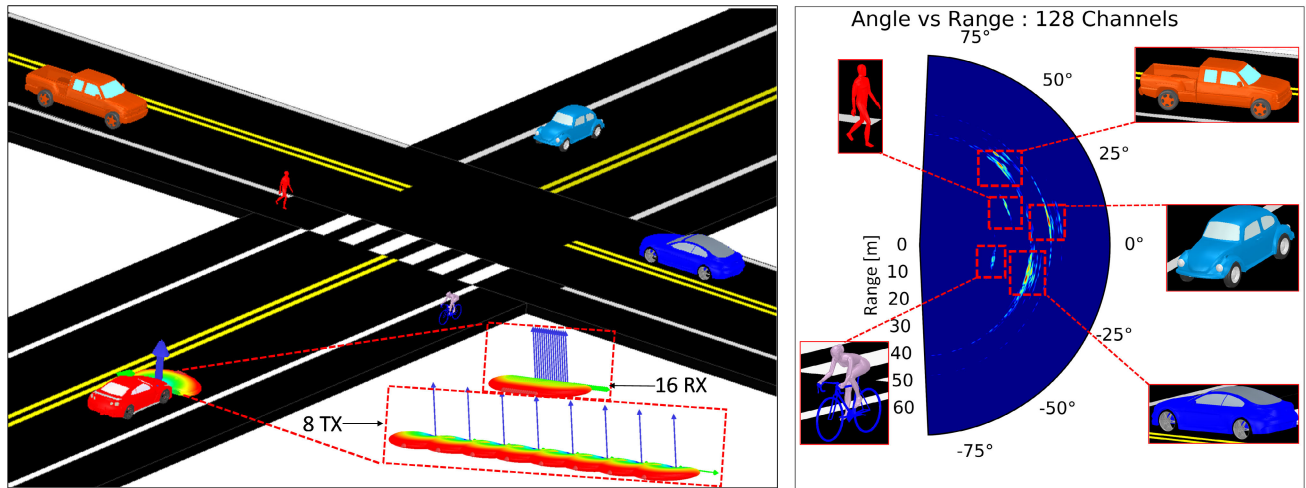
FIGURE 6. Full-scale, high-fidelity physics traffic scene simulation of a MIMO radar sensor and the range-angle map for a 128 MIMO sensor.
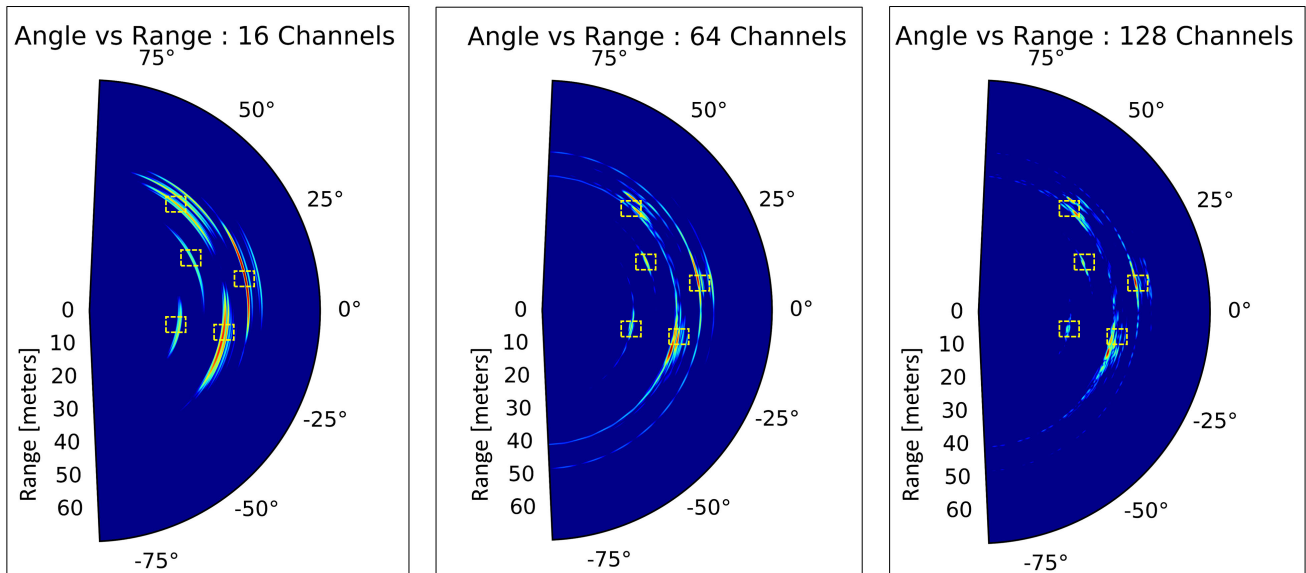

FIGURE 7. Range-angle maps for 16, 64 and 128 channels for the scene shown in Fig.6. The box shaped markers show the actual locations (range and angle) of the targets. Increasing the number of channels improves the DoA estimation resolution.

centers of M_{Tx} antennas. By judiciously spacing the T_x elements, a virtual array can be realized as shown in Fig. 1. Here, using M_{Tx} transmit antennas and N_{Rx} receive antennas, a total of $M_{Tx}N_{Rx}$ virtual channels can be realized. Therefore, in order to realize $M_{Tx}N_{Rx}$ channels, only $M_{Tx} + N_{Rx}$ physical channels are needed for a MIMO scheme. On the other hand, a SIMO scheme would need $1 + M_{Tx}N_{Rx}$ physical channels.

B. FFT BASED POST-PROCESSING FOR DOPPLER AND DIRECTION OF ARRIVAL ESTIMATION

Doppler and angle of arrival were estimated using a FFT scheme as shown in Fig. 2. Synthetic radar returns from

HFSS SBR+ simulations represent antenna-to-antenna (T_x to R_x) coupling in the presence of scatterers. This coupling is presented as the scattered-field S-parameters. Since the solver used for this study is a frequency based solver, each chirp is represented by complex voltage samples of the reflected signals as shown in Fig. 2. A single range profile can be obtained from one chirp by conducting an IFFT across the fast time dimension. In order to obtain separation of targets in Doppler, FFTs were conducted across all chirps in one coherent processing interval (CPI) from a single channel. To achieve this, range profiles from each chirp were loaded into the rows of a Doppler matrix before a second FFT was

TABLE 1. Radar parameters for simulation setup.

Parameter	Value
Center Frequency	77 GHz
Start Frequency	76.625 GHz
Stop Frequency	77.375 GHz
Bandwidth	750 MHz
Maximum Range	70m
Range Resolution	0.2m
Number of gated range bins	350
Velocity Period	80 m/s
Velocity Resolution	0.4 m/s
Pulse Repetition Frequency (PRF)	41.1 KHz
Coherent Processing Interval	4.9ms
Number of pulses	200

carried out along each column. A column in the Doppler matrix represents a single range bin for all the chirps. The second FFT is conducted across all the chirps for each range bin as shown in Fig. 2. Direction of arrival (DoA) estimation was conducted in a similar manner. An IFFT was conducted on the synthetic radar returns of a single chirp from the middle of each channel's CPI. This data was then passed into the rows of a DoA matrix as was done for Doppler. Finally, a second FFT was conducted along each column of this DoA matrix. Each column represents a single range bin for all the channels. Therefore, the second FFT is conducted for each range bin across the channel space.

III. VALIDATION OF SIMULATION SETUP AND POST PROCESSING

A. SIMULATION SETUP

The High Frequency Structure Simulator (HFSS) Shooting and Bouncing Rays (SBR+) solver was used to simulate synthetic radar returns for validation of the MIMO sensor. HFSS SBR+ is an asymptotic, ray tracing electromagnetics solver that efficiently solves electrically large problems. HFSS SBR+ uses geometrical optics (GO) to launch rays from a radiation source. These launched GO rays are vector-field weighted by the radiation pattern or current distribution of the source antenna [34]. HFSS SBR+ then uses physical optics (PO) to 'paint' currents wherever GO rays hit a geometry. Physical theory of diffraction (PTD) wedge corrections and uniform theory of diffraction (UTD) rays are used to account for additional phenomenology due to truncation of PO currents at sharp discontinuities. Finally, HFSS SBR+ also corrects the PO current truncation at shadow boundaries by including creeping wave (CW) physics. Therefore, using GO, PO, UTD, PTD and CW, high-fidelity physics based synthetic radar returns can be obtained [25], [26].

Using 8 T_x elements with a spacing of 8λ and 16 R_x elements with spacing of $\lambda/2$, a 128 virtual channel sensor was designed in SBR+. For each element of the array, the beam-width was 120° and 10° in azimuth and elevation, respectively. An FMCW waveform was used. Table 1 shows the characteristics of the waveform. Since each of the T_x channels are using an identical waveform, orthogonality of T_x waveforms was achieved using a time domain multiplexing (TDM) scheme.
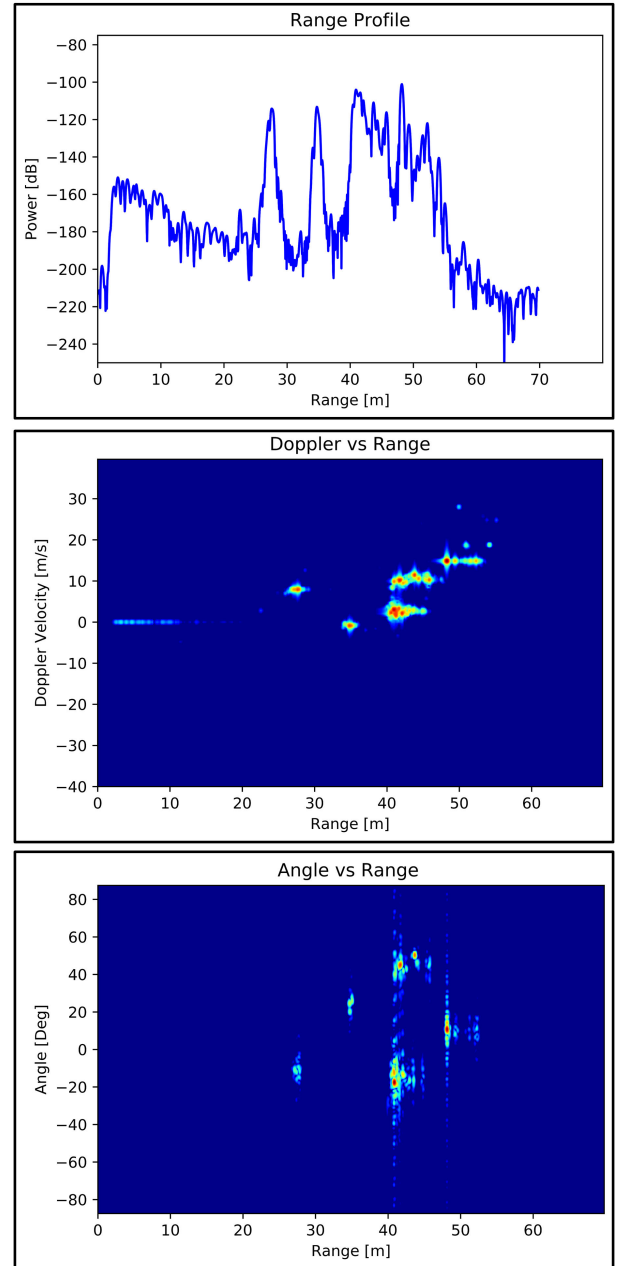

FIGURE 8. Range profile, range-Doppler and rang-angle map for the traffic scene shown in Fig. 6.

B. TEST CASE SCENARIO FOR VALIDATION

In order to validate the virtual MIMO array design, simulation setup and the post processing scheme, three steel plates were placed in front of the MIMO array as shown in Fig. 3. Each of the 3 steel plates had a radar cross section (RCS) of $10m^2$ at 77 GHz. Two plates were placed at angles of 17.3° and −33° at a radial velocity of $10m/s$ with respect to the radar sensor. The third steel plate was placed at bore-sight with a velocity of $-5m/s$. All three targets were placed at a range of $15.3m$ with respect to the radar sensor. The radar platform was stationary ($0m/s$). Since all the steel plates are at the same
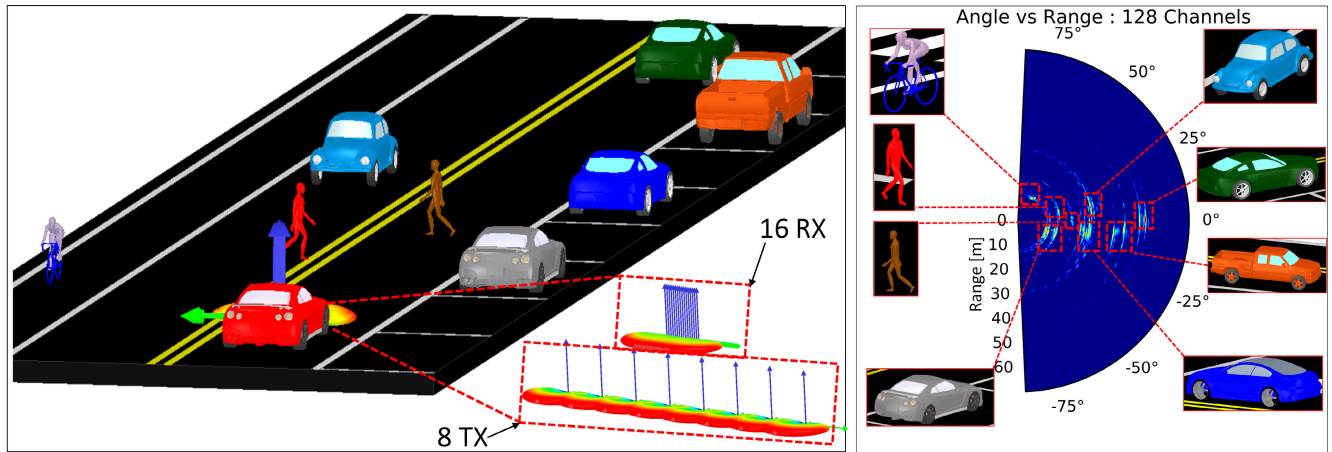
FIGURE 9. Full-scale scene of typical urban driving scenario. The targets in this scene are much closer in angle and range.
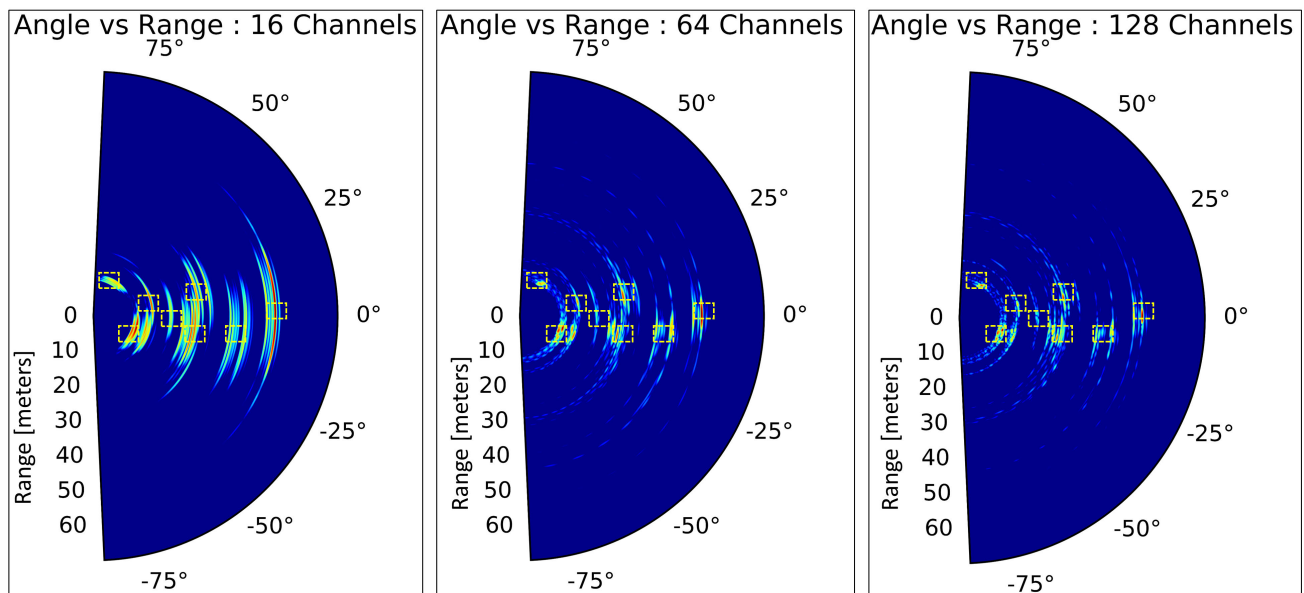

FIGURE 10. Range-angle maps for 16, 64 and 128 channels for the scene shown in Fig.9. The box shaped markers show the actual locations (range and angle) of the targets. Increasing the number of channels improves the DoA estimation resolution.

range, only one target should be resolved in range at 15.3m. On the other hand, only two targets should be resolved in Doppler at -5m/s and 10m/s since two of the targets fall into the same 10m/s velocity bin. Finally, a direction of arrival estimation should resolve all the 3 targets in angle. Fig. 4 shows the range profile, range-Doppler and range-angle map for the setup shown in Fig. 3. All three plots are consistent with the expected results for the arrangement in Fig. 3. In order to test the impact of channel number on the DoA estimation resolution, the DoA estimation was done for 16, 64 and 128 channels. Fig. 5 shows the range-angle maps for 16, 64 and 128 channels. As expected from (5), increasing the number of channels improves the resolution. Specifically, by only using 16 channels and the FFT scheme used here, it is

difficult to differentiate between the peaks corresponding to each plate.

IV. FULL SCALE TRAFFIC SCENE SIMULATION
In order to test the performance of the MIMO sensor in typical traffic scenes, two full-scale scenes were created in HFSS SBR+. Fig. 6 shows a full-scale model of a traffic intersection. The ego vehicle is fitted with an 8 T_x and 16 R_x MIMO sensor. Vehicle bodies were defined as perfect electrical conducting bodies while the windows were defined as a boundary condition that allows rays to be reflected, refracted and transmitted at the air/glass interface (0.25in thick). The road was modelled as an asphalt layered impedance boundary condition. Finally, pedestrians were modelled using the single

material dry skin model [35], [36]. Here, the relative dielectric constant and conductivity are $\epsilon_r = 6.6$ and $\sigma = 38.38$ S/m, respectively.

Fig. 7 shows the range-angle maps for 16, 64 and 128 channels. The range profile, range-Doppler and range-angle maps are shown in Fig. 8. Low fidelity physics simulation techniques use point scatterer models to define the actors in a scene [27]–[33], here we are using realistic, full-scale models of the actors to reveal the accurate distributed nature of real world targets. From Fig. 8, it can be seen that little information of the traffic scene can be deduced from the range profile since some targets exist in the same range bin. The targets can be further separated in Doppler and angle. On the other hand, Fig. 7 shows that the angular resolution improves as the number of channels increases. In Fig. 7, the 16-channel range-angle map shows the targets smeared out in angle. This introduces ambiguity in the actual direction of arrival of a target since it seems to be existing over multiple angle bins. Such ambiguity can worsen when targets are at the same range as shown in Fig. 5. On the other hand, the radar returns of single targets are more localized in angle when 64 and 128-channel sensors are used for the DoA estimation. By inspecting the range-angle maps in Fig. 7, it can be concluded that the 16 channel sensor could still be used for DoA estimation in cases where the targets are widely separated in range and/or angle.

The intersection shown in Fig. 6 is a fairly simple case for DoA estimation. This is because each of the targets are widely spaced in direction of arrival. Furthermore, each of the targets have unobstructed paths between them and the ego vehicle. These factors make it easier for the DoA estimation to isolate the targets in angle. A more complex and critical driving scenario that is representative of typical urban situations is shown in Fig. 9. Here, the targets are close to each other both in range and angle. Furthermore, soft targets like pedestrians have fairly low radar cross section (RCS). This can make it difficult to detect such targets when they are close to high RCS targets such as vehicles. Specifically, the RCS of a pedestrian and a truck can have a relative dynamic range of $20dB$ [7]. Since the targets are closer in range and angle, high angle and range resolutions are needed to be able to isolate the targets. Specifically, assuming a $3m$-wide traffic lane, determination of a clear path up to a range of $50m$ requires a resolution of $3.5°$ [7]. From (5), a 16 channel sensor has a resolution of $7°$ thus making it unfit for such a driving scenario. On the other hand, 64 and 128 channel sensors have resolutions of $1.8°$ and $0.9°$, respectively. Therefore, the performance requirements should still be met by a 64 channel sensor. Fig. 10 shows the range-angle maps obtained from simulating 16, 64 and 128 channel sensors. The range profile, range-Doppler and range-angle maps are for the traffic scene in Fig. 9 are shown in Fig. 11. As shown in Fig. 10, simulation can be used to confirm that a 64 channel sensor meets performance requirements by still being able to resolve the targets in angle. On the other hand, Fig. 10 shows that a 16 channel sensor cannot be reliably used for this type of
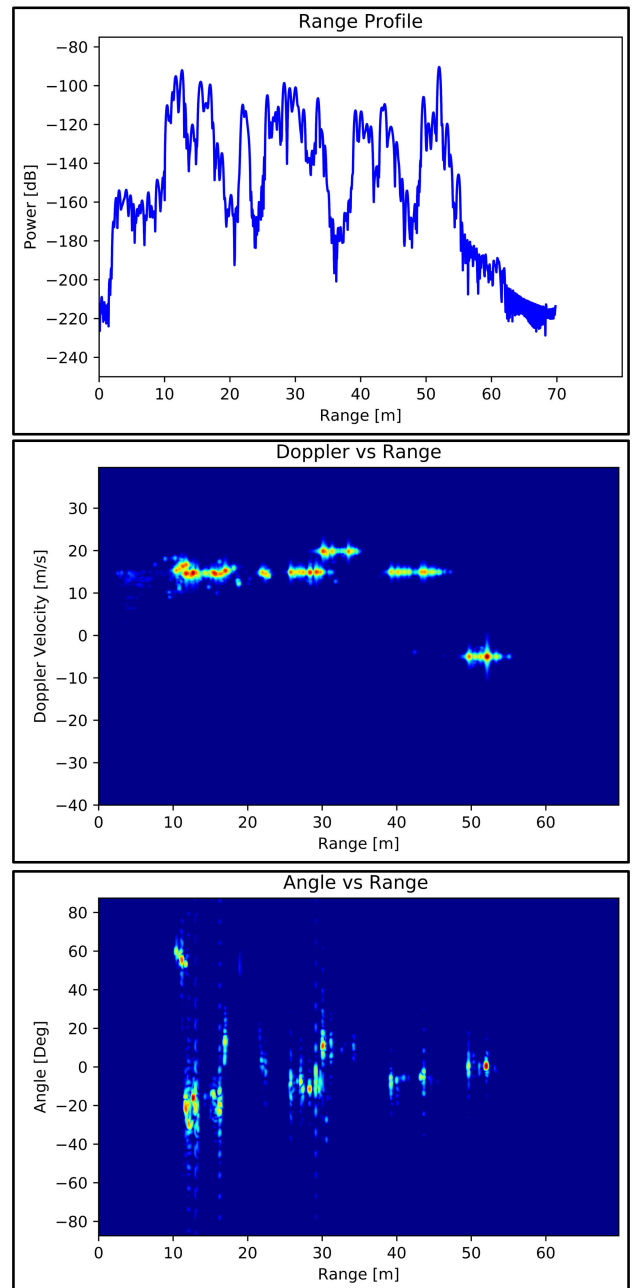

FIGURE 11. Range profile, range-Doppler and rang-angle map for the traffic scene shown in Fig. 9.

driving scenario. This should be compared to the intersection in Fig. 6 where 16 channels were enough to separate the sparsely spaced targets in angle.

V. CONCLUSION

Radar is one of the key sensor technologies for advanced driver assistance systems (ADAS). Using radar, vehicles can simultaneously determine the range, velocity and direction of arrival of multiple targets. For fully autonomous vehicles to be realized, medium and short-range radars will need to operate in crowded urban environments where

high resolution in direction of arrival (DoA) estimation is needed. In order to achieve high DoA resolution, the number of transmitter/receiver channels needs to be increased. Multiple-input/multiple-output (MIMO) schemes are a hardware efficient way of increasing the number of channels in radar sensors. In this paper, we presented a 128 channel MIMO sensor for high resolution DoA estimation. Synthetic radar returns for this MIMO sensor were obtained using high-fidelity physics based electromagnetic simulations of full-scale traffic scenes at 77 GHz. Doppler and DoA were determined using a FFT post processing scheme. DoA estimation using this MIMO sensor was conducted on two full-scale traffic scenes. For each scene, comparisons of performance for 16, 64 and 128 channels were made. A minimum of 16 channels was found to be sufficient for sparsely populated scenarios while 64 channels were necessary for densely populated traffic scenarios. Results from this study show how high-fidelity physics simulations can be used to design and virtually test complex MIMO systems for automotive radar.

REFERENCES

[1] R. H. Rasshofer and K. Gresser, "Automotive radar and lidar systems for next generation driver assistance functions," *Adv. Radio Sci.*, vol. 3, pp. 205–209, May 2005.

[2] D. M. Gavrila, "The visual analysis of human movement: A survey," *Comput. Vis. Image Understand.*, vol. 73, no. 1, pp. 82–98, Jan. 1999.

[3] T. B. Moeslund, A. Hilton, and V. Krügerc, "A survey of advances in vision-based human motion capture and analysis," *Comput. Vis. Image Understand.*, vol. 104, pp. 90–126, Nov./Dec. 2006.

[4] R. Poppe, "Vision-based human motion analysis: An overview," *Comput. Vis. Image Understand.*, vol. 108, nos. 1–2, pp. 4–18, Oct. 2007.

[5] G. Reina, D. Johnson, and J. Underwood, "Radar sensing for intelligent vehicles in urban environments," *Sensors*, vol. 15, no. 6, pp. 14661–14678, Jun. 2015.

[6] S. M. Patole, M. Torlak, D. Wang, and M. Ali, "Automotive radars: A review of signal processing techniques," *IEEE Signal Process. Mag.*, vol. 34, no. 2, pp. 22–35, Mar. 2017.

[7] I. Bilik, O. Bialer, S. Villeval, H. Sharifi, K. Kona, M. Pan, D. Persechini, M. Musni, and K. Geary, "Automotive MIMO radar for urban environments," in *Proc. IEEE Radar Conf. (RadarConf)*, Philadelphia, PA, USA, May 2016, pp. 1–6.

[8] U. Chipengo and M. Commens, "A 77 GHz simulation study of roadway infrastructure radar signatures for smart roads," in *Proc. 16th Eur. Radar Conf. (EuRAD)*, Paris, France, 2019, pp. 137–140.

[9] H. H. Meinel, "Evolving automotive radar—From the very beginnings into the future," in *Proc. 8th Eur. Conf. Antennas Propag. (EuCAP)*, The Hague, The Netherlands, Apr. 2014, pp. 3107–3114.

[10] J. Li and P. Stoica, "MIMO radar with colocated antennas," *IEEE Signal Process. Mag.*, vol. 24, no. 5, pp. 106–114, Sep. 2007.

[11] Z. Zhang, C. Zhou, Y. Gu, and Z. Shi, "FFT-based DOA estimation for coprime MIMO radar: A hardware-friendly approach," in *Proc. IEEE 23rd Int. Conf. Digit. Signal Process. (DSP)*, Shanghai, China, Nov. 2018, pp. 1–5.

[12] E. Fishler, A. Haimovich, R. Blum, D. Chizhik, L. Cimini, and R. Valenzuela, "MIMO radar: An idea whose time has come," in *Proc. IEEE Radar Conf.*, Philadelphia, PA, USA, 2004, pp. 71–78.

[13] S. Lutz, K. Baur, and T. Walter, "77 GHz lens-based multistatic MIMO radar with colocated antennas for automotive applications," in *IEEE MTT-S Int. Microw. Symp. Dig.*, Montreal, QC, Canada, Jun. 2012, pp. 1–3.

[14] S. Suleymanov, "Design and implementation of an FMCW radar signal processing module for automotive applications," M.S. thesis, Univ. Twente, Enschede, The Netherlands, Aug. 2016.

[15] J. J. M. de Wit, W. L. van Rossum, and A. J. de Jong, "Orthogonal waveforms for FMCW MIMO radar," in *Proc. IEEE RadarCon (RADAR)*, Kansas City, MO, USA, May 2011, pp. 686–691.

[16] F. C. Robey, S. Coutts, D. Weikle, J. C. McHarg, and K. Cuomo, "MIMO radar theory and experimental results," in *Proc. 38th Conf. Rec. Asilomar Conf. Signals, Syst. Comput.*, Pacific Grove, CA, USA, 2004, pp. 300–304.

[17] A. Haimovich, R. Blum, and L. J. Cimini, "MIMO radar with widely separated antennas," *IEEE Signal Process. Mag.*, vol. 25, no. 1, pp. 116–129, Dec. 2008.

[18] J. Wenger, "Automotive radar–status and perspectives," in *Proc. IEEE Compound Semiconductor Integr. Circuit Symp. (CSIC)*, Palm Springs, CA, USA, Oct. 2005, p. 4.

[19] J. Hasch, R. Topak, T. Schnabel, T. Zwick, R. Weigel, and C. Waldschmidt, "Millimeter-wave technology for automotive radar sensors in the 77 GHz frequency band," *IEEE Trans. Microw. Theory Techn.*, vol. 60, no. 3, pp. 845–859, Jan. 2012.

[20] K. Ohguchi, M. Shono, and M. Kishida, "79 GHz band ultra-wideband automotive radar," *Fujitsu Ten Tech. J.*, vol. 39, pp. 9–14, 2013.

[21] J. Singh, B. Ginsburg, S. Rao, and R. Ramasubramanian, "AWR1642 mmWave sensor: 76-81-GHz radar-on-chip for short-range radar applications," Texas Instrum., Dallas, TX, USA, Tech. Rep., 2017, pp. 1–7. [Online]. Available: https://www.ti.com/lit/wp/spyy006/spyy006.pdf

[22] B.-H. Ku, P. Schmalenberg, O. Inac, O. D. Gurbuz, J. S. Lee, K. Shiozaki, and G. M. Rebeiz, "A 77-81 GHz 16 element phased array receiver with ±50° beam scanning for advanced automotive radars," *IEEE Trans. Microw. Theory Techn.*, vol. 62, no. 11, pp. 2823–2832, Nov. 2014.

[23] *Implementing Digital Processing for Automotive Radar Using SoCs*, Altera, San Jose, CA, USA, 2013, pp. 1–15.

[24] Ohnsman, Forbes. (Oct. 2016). *Toyota's Robot-Car Line In The Sand: 8.8 Billion Test Miles To Ensure Safety*. [Online]. Available: https://www.forbes.com/sites/alanohnsman/2016/10/03/toyotas-robot-car-line-in-the-sand-8-8-billion-test-miles-to-ensure-safety/#4ef4269316f0

[25] U. Chipengo, P. M. Krenz, and S. Carpenter, "From antenna design to high fidelity, full physics automotive radar sensor corner case simulation," *Model. Simul. Eng.*, vol. 2018, pp. 1–19, Dec. 2018.

[26] A. P. Sligar, "Machine learning-based radar perception for autonomous vehicles using full physics simulation," *IEEE Access*, vol. 8, pp. 51470–51476, 2020.

[27] D. Belgiovane and C.-C. Chen, "Micro-Doppler characteristics of pedestrians and bicycles for automotive radar sensors at 77 GHz," in *Proc. 11th Eur. Conf. Antennas Propag. (EUCAP)*, Mar. 2017, pp. 2912–2916.

[28] M. S. Seyfioglu, B. Erol, S. Z. Gurbuz, and M. G. Amin, "DNN transfer learning from diversified micro-Doppler for motion classification," *IEEE Trans. Aerosp. Electron. Syst.*, vol. 55, no. 5, pp. 2164–2180, Oct. 2019.

[29] J. M. Garcia-Rubia, O. Kilic, V. Dang, Q. M. Nguyen, and N. Tran, "Analysis of moving human micro-Doppler signature in forest environments," *Prog. Electromagn. Res.*, vol. 148, pp. 1–14, Jun. 2014.

[30] H. Yan, W. Doerr, A. Ioffe, and H. Clasen, "Micro-Doppler based classifying features for automotive radar VRU target classification," in *Proc. 25th Int. Tech. Conf. Enhanced Saf. Vehicles (ESV)*, Detroit, MI, USA, 2017, pp. 1–8.

[31] T. Johansson, A. Anderson, M. Gustafsson, and S. Nilsson, "Positioning of moving non-line-of-sight targets behind a corner," in *Proc. 13th Eur. Radar Conf.*, London, U.K., Oct. 2016, pp. 181–184.

[32] T. Schipper, J. Schlichenmaier, D. Ahbe, T. Mahler, J. Kowalewski, and T. Zwick, "A simulator for multi-user automotive radar scenarios," in *IEEE MTT-S Int. Microw. Symp. Dig.*, Apr. 2015, pp. 1–4.

[33] L. Huang, H. Chen, and J. Bai, "Simulation of the effect of signal source's phase noise on millimeter wave automotive radar system based on SystemVue," in *Proc. IEEE Int. Workshop Electromagn., Appl. Student Innov. Competition (iWEM)*, May 2016, pp. 1–3.

[34] *HFSS SBR+ Technical Overview*, Ansys Electron, Canonsburg, PA, USA, 2020 R1, 2020.

[35] T. Wu, T. S. Rappaport, and C. M. Collins, "The human body and millimeter-wave wireless communication systems: Interactions and implications," in *Proc. IEEE Int. Conf. Commun. (ICC)*, Jun. 2015, pp. 1–7.

[36] D. Belgiovane, C.-C. Chen, M. Chen, S. Y.-P. Chien, and R. Sherony, "77 GHz radar scattering properties of pedestrians," in *Proc. IEEE Radar Conf.*, May 2014, pp. 735–738.

USHEMADZORO CHIPENGO (Student Member, IEEE) received the B.S. degree in electrical engineering from the University of Nicosia, Cyprus, in 2013, and the M.Sc. and Ph.D. degrees in electrical engineering from The Ohio State University, in 2017.

With a focus on electromagnetics, he has conducted research on slow wave structures for high power microwave sources, antennas, microwave circuits and computational electromagnetics. He joined Ansys Inc., in 2017, where he is currently a Senior Application Engineer. He uses his expertise in simulation to solve a wide range of electromagnetics problems. His current research interests include slow wave structures for high-power microwave sources, antenna design for automotive applications (V2V, V2I, 5G, RKE, Satellite radio etc.), and automotive radar for advanced driver assistance systems (ADAS).

ARIEN SLIGAR received the B.S. and M.Sc. degrees in electrical engineering from Oregon State University, in 2004 and 2006, respectively, with a focus on electromagnetics and microwave components.

He joined Ansys Inc., in 2006, where he is currently a Principal Engineer, focusing on advanced applications of numerical simulation for electromagnetics and electronics. He is an Expert in the application of electromagnetic field simulation to the design of antennas, complex antenna systems, microwave components, and high-speed electronics. He works with leading technology companies and provides engineering guidance allowing them to successfully apply simulation and automated workflows to their most difficult design challenges.

SHAWN CARPENTER received the B.E.E. degree in electrical engineering from the University of Minnesota Institute of Technology, in 1988, and the M.S.E.E. degree in electrical engineering from Syracuse University, in 1991, concurrently with the General Electric Thomas Edison Advanced Course in Engineering program.

He was a Senior Microwave Engineer in module design and array technology with the GE Aerospace Electronics Laboratory (Syracuse, NY, USA), VP Sales and Marketing for Sonnet Software, Inc., and the Director of Sales and Marketing with Delcross Technologies. He joined Ansys Inc., in 2015, during the acquisition of Delcross Technologies, where he is currently a Senior Product Manager with the Ansys Electronic Business Unit and the Program Director of 5G. His current interests include phased array modeling techniques for MIMO and adaptive beamforming, installed antenna-host interactions, mm-wave radar sensor modeling, and physical channel modeling for electrically large environments.

• • •